Binding at the Core. Computational Study of Structural and Ligand Binding Properties of Naphthyridine-Based Dendrimers

Paola Posocco, Marco Ferrone, Maurizio Fermeglia, and Sabrina Pricl*

Molecular Simulations Engineering (MOSE) Laboratory, Department of Chemical Engineering (DICAMP), University of Trieste, Piazzale Europa 1, 34127 Trieste, Italy

Received November 13, 2006; Revised Manuscript Received January 12, 2007

ABSTRACT: In this work, we studied the effect of connecting units in three generations of two series of dendritic molecules on the structural properties and the complexation behavior based on hydrogen bonding between the dendrimer cores and two different guest molecules. Our molecular simulations revealed that the geometry of the core strongly influences the generational growth of these macromolecules, ultimately resulting in similar, flower-like, shape-consistent macromolecular hosts. The calculations of the free energies of binding between all dendrimers and their guests, obtained by applying the so-called MM/PBSA methodology, are in utter agreement with the corresponding experimental values. Host−guest interactions and clathration in a dendritic architecture are intriguing properties of dendrimers, especially when the location of the guest molecules can be controlled and predetermined by the incorporation of specific binding sites utilizing hydrophobic interactions, hydrogen-bonding, or a metal ion coordination site.

Introduction

Since the pioneering work of well-defined, three-dimensional structural ordered macromolecules by Vögtle,[1] Tomalia,[2,3] and Newkome,[4] interest in dendrimers (and hyperbranched polymers) has been increasing at an amazing rate. The term *dendrimer* (deriving from the Greek words *dendra* = tree and *meros* = part) aptly describes the structure of this new class of macromolecules that possess highly branched, three-dimensional, regular tree-like features.[5] A typical dendrimer presents three distinguishing architectural areas: (a) a polyfunctional central core or focal point, (b) an interior consisting of repeat units of varying number (the so-called *generations G*), radially attached to the core itself, and (c) exterior terminal groups attached at the outermost positions (see Figure 1).

For the synthesis of these compounds, one may view those processes as simply sequentially staged, quantized polymerization events. The assembly of reactive monomers,[6] branch cells,[7,8] or dendrons[9] around atomic or molecular cores produce dendrimers according to *divergent* or *convergent* dendritic branching principles. The most obvious difference between the two approaches is in the direction of dendrimer growth. In divergent synthesis, dendrimer growth starts from a polyfunctional core and proceeds radially outward with the stepwise addition of successive layers of building blocks. In convergent synthesis, dendrimer growth begins at the chain ends and proceeds inward through successive additions of the growing dendritic molecules to a single monomer unit. In either way, such systematic filling of space around cores with branch cells as a function of generational growth stages to give discrete, quantized bundles of mass has shown to be mathematically predictable.[10] Thus, compared with traditional linear polymers, dendrimers possess tailored structures, an almost single molecular weight rather than a distribution of molecular weights, and a multiplicity of controllable functional groups at their periphery. Further, in most cases, the construction of a sharply controlled microenvironment around functional sites in linear polymer is nearly impossible due to the entanglement properties of polymer chains. In other words, dendrimers may provide a new, controlled "place of chemical and physical events", and opportunities required for achievement of high selectivity, high efficiency, high recognition, and other functionalities. The characteristic features of application-oriented dendrimers are highlighted in Figure 1; accordingly, a plethora of exploitations of this macromolecular class is currently being considered for both materials and life science applications, including catalyst particles[11] and nanoscale reactors,[12] micelle mimicry,[13] drug delivery systems,[14] magnetic resonance imaging agents,[15] immunodiagnostic devices,[16] and gene therapy vectors,[17] synthetic mimicry of protein active sites,[18] energy funnels,[19] and building blocks for more elaborate supermolecular structures,[20] just to name a few.

Shape and multiplicity of the core (N_c) and branching multiplicity (N_b), as well as the size and shape of the end groups, in addition to their chemical composition, determine the chemical and physical properties of a given dendrimer family. Controllable surface functionalization of dendrimers can provide segregated properties between surface and interior; thus, a dendrimer could function as a unimolecular *endoreceptor*, manifesting noncovalent chemistry reminiscent of traditional, regular and inverse micelles, or liposomes, if binding groups are located in its interior. Conversely, when binding functionalities are located at the dendrimer periphery, dendrimers can work as *nanoscaffolding*, exhibiting a high propensity to cluster or complex in an *exoreceptor* fashion with a variety of (bio)-macromolecules and metals.

One of the most characteristic features of high-generation dendrimers is that they generally adopt a roughly globular shape in solution, characterized by the presence of cavities and voids, which in turn depend on the chemical composition, flexibility, and number of branching arms at junction points. The internal cavity of an appropriately designed dendrimeric structure could be then used to encapsulate guest molecules. Basically, two strategies are available for small compound encapsulation in dendrimers. The first is physical encapsulation, according to which a trapped molecule is no longer able to diffuse out of

* Corresponding author. E-mail: sabrina.pricl@dicamp.units.it. Telephone: +390405583750.Fax: +39040569823.

10.1021/ma062610a CCC: $37.00
Published on Web 02/13/2007

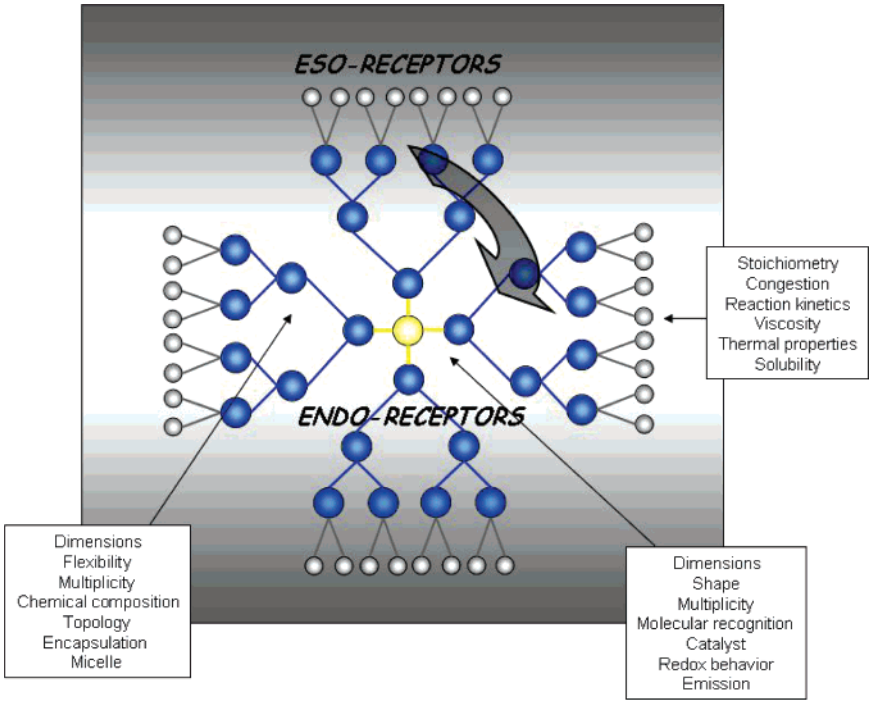

Figure 1. Schematic representation of properties of dendrimers and their potentials as functional materials.

the *dendritic box*, as the macromolecule outer layer is capped with bulky, sterically crowded functional groups, eventually subjected to hydrogen bonding.[21] The second strategy for the encapsulation of guest molecules in a dendrimer host is based on multiple noncovalent chemical interactions, such as hydrogen bonding and/or hydrophobic interactions, between the host and its guest(s).[22] Moreover, in contrast to the nonspecific physical entrapment of guest molecules within the dendritic branches, the location of the guest compounds can be controlled by the incorporation of specific binding sites.

In this perspective, Zimmerman et al.[23] have recently studied the effect of connecting units in the dendritic molecules on the complexation behavior based on hydrogen bonding between the core and guest molecules. To this purpose, they synthesized two different types of dendrimers up to a third generation, characterized by a naphthyridine unit as a core (see Figure 2a) and using the two benzamidinium compounds **c** (3,5-di(tert)-butylbenzamydine) and **d** (3,5-di(3′,5′-di(*tert*)butylphenyleth-ynyl)benzamydine) as guests (see Figure 2b). Dendrimers **a** and **b** differ only in the two atoms connecting the aryl groups in the interior: the $-OCH_2-$ groups characterizing the dendrimer family **b** are polar and flexible, whereas the phenyl-acetylene units are apolar and likely make dendrimer family **a** quite porous.

For both families, the authors[23] found that the guest molecules were trapped at the naphthyridine core by hydrogen bonding, and the stoichiometry of all complexes was determined to be 1:1. The binding constant between the all dendritic hosts and their guest were very close to those of a nondendritic naph-thyridine core, indicating that the size of the dendrimers and its chemical nature only marginally alter the relevant com-plex stability, and principally, the nature of the core is effective in the complex formation. Only with the larger compound **d**, the higher-generation dendrimer hosts bind more weakly, possibly reflecting the increased steric demands for complex-ation.

To verify all of this evidence and to clarify the host/guest interactions from a molecular standpoint, in this work, we

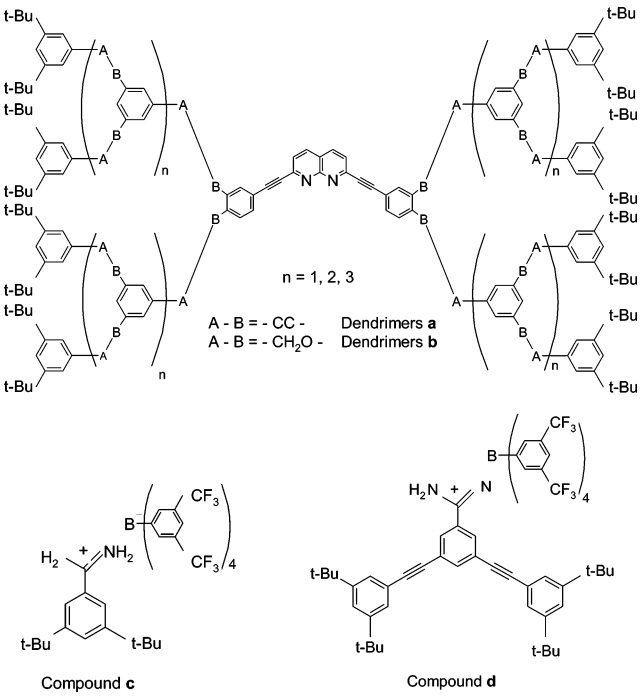

Figure 2. (a, top) Dendritic molecules capable to bind guest compounds (b, bottom) at their core.[23]

applied different computer molecular simulation techniques to (i) characterize the structural features of dendrimer families **a** and **b** and (ii) calculate the free energy of binding of **a** and **b** with their guest **c** and **d**. Molecular dynamics simulations in explicit solvent were performed to obtain molecular dimensions, shapes, internal void, and fractal characteristics as functions of dendrimer type and generations. The so-called molecular mechanics/Poisson−Boltzmann surface area (MM/PBSA) meth-odology, originally devised by Peter Kollman and his group,[24] was employed to estimate the total free energy of binding ΔG_{BIND} (and its components) between all dendrimers and their guests.

Computational Details

All simulations were performed using the program packages Materials Studio (version 2.2, Accelrys, San Diego,USA) and AMBER 7.[25,26]

The model structures of the dendrimer series **a** and **b** (up to $G = 3$) were generated using the Polymer/Dendrimer Builder module of Materials Studio. Geometry refinement was carried out using the Sander module of AMBER 7 via a combined steepest descent−conjugate gradient algorithm, with the parm99EP version of the AMBER force field,[27] setting as convergence criterion for the algorithm the root-mean-square of the Cartesian elements of the energy gradient equal to 10^{-4} kcal/(mol Å). Eventual missing force field parameters for inhibitors were generated as follows: AM1[28] geometry optimization of the structure was followed by RHF/6-31G* single-point calculation to obtain the electrostatic potentials. Next, the restrained potential (RESP) method[29] was used for charge fitting. The missing bonds, angle torsions, or van der Waals parameters not included in the parm99EP force field were transferred from the newly developed general AMBER force field (GAFF).[30] The conformational search was carried out using a well-validated, combined molecular mechanics/molecular dynamics simulated annealing (MDSA) protocol.[31−34] Accordingly, the relaxed structures were subjected to five repeated temperature cycles (from 300 to 1000 K and back) using constant volume/constant temperature (*NVT*) MD conditions. At the end of each annealing cycle, the structures were again energy minimized to converge below 10^{-4} kcal/(mol Å), and only the structures corresponding to the minimum energy were used for further modeling. The same procedure was applied for obtaining the 3D molecular models of the two hosts **a** and **b**.

The details of the isolated dendrimer structures at 300 K have been obtained by performing extensive MD simulations in the canonical (*NVT*) ensemble. The GB/SA implicit solvent model[35] was used to mimic the corresponding experimental solvated environment.[23] Each dendrimer molecule was gradually heated to 300 K in three intervals, allowing a 50 ps interval per each 100 K, and then equilibrated for 1 ns at 300 K. A further 3 ns of MD data collection run was then carried out. The calculation of molecular surfaces for all generations was performed using the Connolly[36−38] and solvent-accessible[5,40−41] algorithms.

In the case of the host−guest complexes, each molecular assembly was refined in the AMBER suite using the quenched molecular dynamics method (QMD).[34,41−45] In this case, 1 ns MD simulation at 300 K was employed to sample the conformational space of each dendrimer−ligand complex in the GB/SA continuum solvation environment. The integration step was equal to 2 fs. After each 100 ps, the system was cooled to 0 K, the structure was extensively minimized, and then stored. The best energy configuration of each complex resulting from the previous step was solvated in a box of a mixture of 10% CH_3-CN and 90% $CHCl_3$ molecules.[23] Periodic boundary conditions were applied, with constant pressure conditions and a coupling constant of 0.2 ps. All optimized systems were then subjected to gradual heating, following the same procedure described for the isolated dendrimer molecules. Productive *NPT* MD runs were carried out for 500 ps, and the relevant trajectory frames were saved every 10 ps. An integration time step of 2 fs was adopted, together with constant temperature conditions with separate solute−solvent coupling factors of 0.2 and 0.1 ps, respectively.

The binding free energy ΔG_{BIND} of each complex in solvent was estimated via the widely used molecular mechanics/Poisson−Boltzmann surface area (MM/PBSA) methodology.[24] According to this approach, ΔG_{BIND} can be calculated from computational analysis of a single simulation of each host−guest complex and includes explicit computed components corresponding to "gas-phase" dendrimer−ligand interactions (ΔE_{MM}), conformational entropy ($T\Delta S$), and solvation contributions (ΔG_{SOLV}):

$$\Delta G_{BIND} = \Delta E_{MM} + \Delta G_{SOLV} - T\Delta S \quad (1)$$

The term ΔE_{MM} in eq 1 can be further split into contributions from electrostatic (ΔE_{ELE}^{MM}) and van der Waals (ΔE_{vDW}^{MM}) energies:

$$\Delta E_{MM} = \Delta E_{ELE}^{MM} + \Delta E_{vdW}^{MM} \quad (2)$$

The solvation free energy, ΔG_{SOLV}, can in turn be expressed as the sum of an electrostatic component, ΔG_{ELE}^{SOLV}, and a nonpolar contribution, ΔG_{NP}^{SOLV}:

$$\Delta G_{SOLV} = \Delta G_{ELE}^{SOLV} + \Delta G_{NP}^{SOLV} \quad (3)$$

ΔG_{ELE}^{SOLV} was calculated by solving the finite-difference Poisson−Boltzmann equation using the Delphi package,[46] with interior and exterior dielectric constants equal to 1 and 38, respectively. A grid spacing of 2/Å, extending 20% beyond the dimensions of the solute, was employed. The nonpolar component in eq 3 was obtained from the solvent-accessible surface area (SASA) using the following empirical relationship: $\Delta G_{NP}^{SOLV} = \gamma SASA + \beta$, in which $\gamma = 0.00542$ kcal/(mol Å^2) and $\beta = 0.92$ kcal/mol. The calculation of molecular surface areas, the solvent accessible surfaces, and the associated volumes was performed using the MSMS program.[47] Each measure of surface/volume is averaged over the equilibrated structures extracted from the corresponding MD trajectory.

Normal-mode analysis was applied to estimate the configurational/conformational entropy component $T\Delta S$ in eq 1.[48] On the basis of MD snapshots of each complex, we generated structures of the uncomplexed species by removing the atoms of the dendrimer host and the molecular guest, respectively. Each of those structures was minimized using a distance-dependent dielectric constant $\epsilon = 4r$ to account for solvent screening, and its entropy was calculated using classical statistical formulas and normal-mode analysis. To minimize the effects due to different conformations adopted by individual snapshots, we averaged the estimation of entropy over 10 snapshots.

Results and Discussion

Analysis of Dendrimer Classes a and b. The equilibration of the *NVT* MD for each dendrimer generation *G* was monitored through the potential energy E_p and the radius of gyration R_g. Smaller generations equilibrated fast, family **a** being characterized by stiffer branches and, hence, slightly faster equilibrations at higher *G*. However, *G*-3 of **b** was also well stabilized within the first 1 ns. The extent of the relaxation of dendrimer molecules was determined from the autocorrelation function of the squared radius of gyration $C_{R_g}(t)$ (see Figure 3) given by the following relationship:

$$C_{R_g}(t) = \frac{\langle (R_g^2(t) - \langle R_g^2 \rangle)(R_g^2(0) - \langle R_g^2 \rangle) \rangle}{\langle R_g^4 \rangle - \langle R_g^2 \rangle^2} \quad (4)$$

The corresponding relaxation times t_{R_g} (with $C_{R_g}(t_{R_g}) = 1/e$) are reported in Table 1, from which we can safely conclude

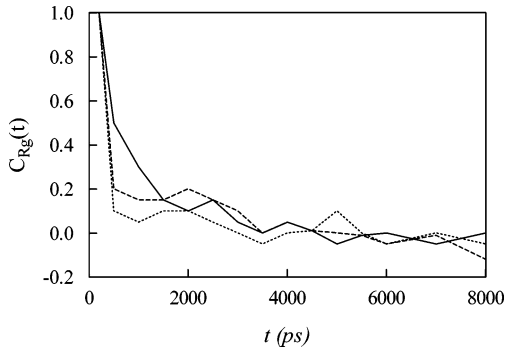

Figure 3. Autocorrelation function of the squared radius of gyration for dendrimers **a**: (···), *G*-1; (− − −), *G*-2; (——), *G*-3.

Table 1. Properties of Dendrimers a and b by Generation[a]

dendrimer	*Z*	M_w	*N*	t_{R_g} (ps)	R_g (nm)
G-1**a**	8	2430	376	433	1.44
G-2**a**	16	4929	670	401	1.81
G-3**a**	32	9928	1528	399	2.46
G-1**b**	8	2501	400	378	1.33
G-2**b**	16	5097	816	386	1.68
G-3**b**	32	10 288	1648	412	2.48

[a] Z = number of terminal groups, M_w = molecular weight; N = number of atoms; t_{R_g} = relaxation time; R_g = radius of gyration.

that the simulation times employed (4 ns) are long enough to sample enough independent configurations for sufficient averaging of the static properties. Moreover, we did not find any apparent dependence of the relaxation time on the generation numbers and only a slight difference between the two families, mainly ascribable to the difference in branch flexibility, as highlighted above.

Figure 4 shows the molecular models of generations 1, 2, and 3 for each dendrimer family **a** and **b**, taken from the equilibrated trajectory of the corresponding MD *NVT* simulations. Interestingly, a central cavity of characteristic dimensions of about 13 Å is generated and maintained near the naphthyridinic core for both dendrimer classes and generations, suitable for guesting a small molecule (vide infra).

As is apparent from Figure 4, the overall molecular shape for the three generations of **a** and **b** is somewhat similar. Both equilibrium *G*-1 conformers of **a** and **b** tend to adopt a "false-propeller" structure, where one of the branches has a torsion angle that is opposite in sign, although similar in amplitude, and this conformation remains stable throughout the relevant simulations. From this structure, with largely separated and weakly interacting branches, the dendrimers progressively evolve toward a conformation in which two dimensions prevail over the third. Accordingly, the molecules of *G*-2 and *G*-3 tend to assume a flowerlike form in which one side, the one where the branches protrude from, exposes a highly irregular and fringed surface, whereas the other one is rather flat. An utterly analogous behavior, characterized by shape persistency, has already been reported for poly(phenylene)-based dendrimers, characterized by a core featuring a benzene ring from which branches bearing a triple C≡C bond emanates.[33,39,40]

The dendrimer size can be quantified by considering the values of the radius of gyration R_g of the molecular structure, defined as:

$$R_g = \left(\frac{\sum_i |r_i - r_0|^2 m_i}{\sum_i m_i} \right)^{1/2} \tag{5}$$

$$S = \begin{bmatrix} \overline{(x_i - x_0)^2} & \overline{(x_i - x_0)(y_i - y_0)} & \overline{(x_i - x_0)(z_i - z_0)} \\ \overline{(x_i - x_0)(y_i - y_0)} & \overline{(y_i - y_0)^2} & \overline{(y_i - y_0)(z_i - z_0)} \\ \overline{(x_i - x_0)(z_i - z_0)} & \overline{(y_i - y_0)(z_i - z_0)} & \overline{(z_i - z_0)^2} \end{bmatrix} \tag{6}$$

$$x_0 = \frac{\sum_i m_i x_i}{\sum_i m_i} \qquad y_0 = \frac{\sum_{i=1} m_i y_i}{\sum_i m_i} \qquad z_0 = \frac{\sum_{i=1} m_i z_i}{\sum_i^N m_i} \tag{7}$$

where m_i is the mass of atom i, $r_i = r_i(x_i, y_i, z_i)$ the position of atom i , and $r_0 = r_0(x_0, y_0, z_0)$ the position of the center of mass of the molecule. According to its definition, (i.e., the square root of the second invariant of tensor S, eq 6), R_g accounts for the spatial distribution of the atom chains by mediating over all N molecular components. The R_g values estimated by MD simulations for all generations of the two series of dendrimers are listed in Table 1, while Figure 5a shows the behavior of R_g as a function of the dendrimers molecular mass M_w in logarithmic scale (see below).

Fractal geometry is a mathematical tool for dealing with complex systems that have no characteristic length scales. Scale-invariant systems are usually characterized by noninteger (i.e., fractal) dimensions, and hence the goal of any fractal analysis is to find a relationship of some kind of power-law

$$\text{physical property} \sim \text{variable}^{\text{ scaling exponent}} \tag{8}$$

where the variable and the exponent are related to the fractal dimension. This relation is obviously one that can cover a very broad range of molecular structures and different physical properties; however, this kind of power-law requires some symmetry in the structure. A common scale exponent may exist for a given property of a series of different homologous molecules (not necessarily setting a fractal dimension) or for a topological property of a single molecule that displays fractal characteristics.

The linear relation between log R_g and log M_w is an indication for a space-filling structures and the related (eq 8) fractal dimensionality d_c takes account of the compactness of the dendrimers serie (d_c is about 2.4 in the case of dendrimers **a**, and 2.6 in the case of dendrimers **b**, respectively (vide infra))).

A further grasp of the structure-persistent characteristics of these dendrimers can be obtained by considering the average values of the three principal moments of inertia I_z, I_y, I_x, where I_z, I_y, I_x represent the eigenvalues of the moment of inertia tensor in descending order. Figure 5b shows the average aspect ratios I_z/I_x and I_z/I_y for the three generations of dendrimers **a** and **b**. Interestingly, both **a** and **b** maintain approximately constant values of the aspect ratios I_z/I_x and I_z/I_y, a clear indication of shape persistency. The persistence in shape is also reflected on the relative shape anisotropy, which is defined as:[51]

$$k = 1 - \frac{3\langle I_2 \rangle}{\langle I_1^2 \rangle} \tag{9}$$

where I_1 and I_2 are the first and second invariants of the radius of gyration tensor:

$$I_1 = I_x + I_y + I_z$$
$$I_2 = I_xI_y + I_yI_z + I_xI_z \quad (10)$$

Clearly, this quantity assumes values between 1 (for a linear array of atoms) and 0 (for shapes characterized by high 3D similarity). Figure 5c reveals that the relative shape anisotropy of all simulated dendrimers is not close to zero, so these molecular families are still far from adopting compact, spherical structures.

The main difference between the two classes of dendrimers appears to arise at generation 3. Because of the rigid triple bond, structures of group **a** are less compact than structures of group **b** at the first two generations; at generation 3, the larger number of conformational degrees of freedom equilibrates the overall effect of the different rigidity at the local level, as visibly appears in both parts c and d of Figure 5, where R_g and M_w have been normalized using the corresponding values for generation 1 (indicated as $R_g(1)$ and $M_w(1)$, respectively).

Surface representations of macromolecules, and especially of dendrimers, have been proven to be a useful tool for characterizing the structure, interactions, and properties of such compounds. In particular, a quantitative analysis of the internal surface area and solvent-filled volume can be made by resorting to the concept of *solvent accessible surface area (*SASA).[39,40] The SASA is obtained by "rolling" a sphere of radius r_p around the van der Waals surface of the molecule, where r_p represents the effective radius of the solvent (e.g., $r_p = 1.4$ Å for a water molecule). The SASA is then composed of the locus of the probe−sphere midpoints. In principle, the surface area of an ideal, spherical molecule containing no internal voids can be defined as:

$$\mathrm{SASA} = 4\pi\,(R + r_p)^2 \quad (11)$$

in which R and r_p are the radius of the spherical molecule and the probe, respectively. Accordingly, a plot of $(\mathrm{SASA})^{1/2}$ versus r_p for such an ideal molecule would be linear, with a slope of $2\sqrt{\pi}$ and intercept proportional to the radius R. Typically, real molecules are never exactly spherical, nor free from internal voids. Therefore, for large values of r_p, SASA is expected to reveal a first-order dependence from r_p, whereas for small values of the probe radius, a deviation from linearity associated with the internal region can be predicted.

Parts a and b of Figure 6 show the plots of $(\mathrm{SASA})^{1/2}$ versus r_p for the three generations of the two classes of dendrimers **a** and **b**.

As can be seen in Figure 6, for large values of r_p, SASA indeed becomes linear with r_p for both dendrimer families, as expected; nevertheless, for small probe radii, a positive deviation from linearity is observed, owing to the extra surface area associated with the interior regions of the molecules. The linear regression analysis of data in Figure 6 indicates both the amount of any internal surface area (A_{int}) and the size (i.e., the diameter) d_{SASA} of each dendrimer (see Table 2). As we can see, for both molecular families, the internal surface area A_{int} increases from approximately 13−15% for *G*-1 to almost 30−50% for *G*-3. This behavior is reminiscent of that exhibited by rather different series of dendrimers, such as poly(propylene imine),[52] phenylene-based,[33] and poly(ether)-based dendrimers.[5]

A measure of the volume associated with the internal cavities of the dendrimers, V_{int}, can be achieved analyzing the behavior of the volume contained within the calculated SASAs, V_{SASA}, again as a function of the probe radius r_p. Reconsidering the example of the ideally spherical molecule, devoid of internal cavities, the volume contained within the SASA of the sphere is given by the following relationship:

$$V_{\mathrm{SASA}} = {}^4/_3\pi\,(\mathrm{R} + r_p)^3 \quad (12)$$

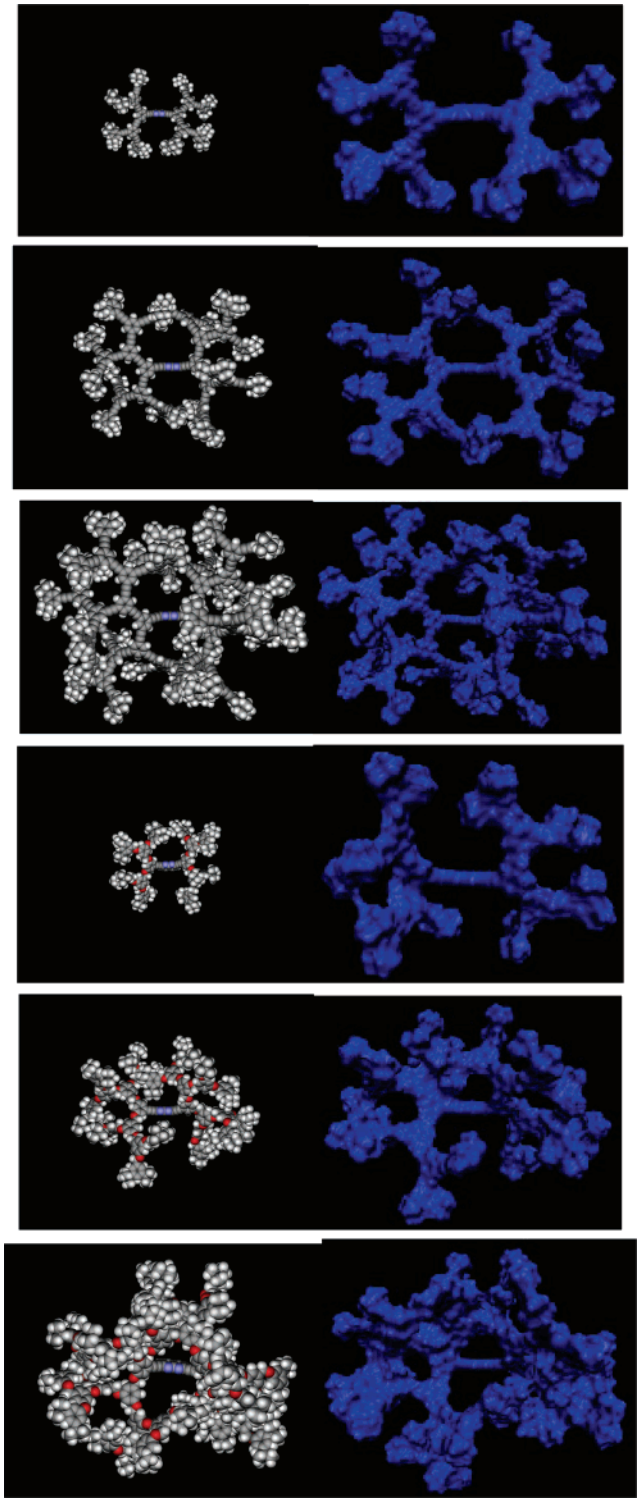

Figure 4. Molecular models taken from equilibrated NVT MD snapshots for dendrimers **a** (upper three panels) and dendrimers **b** (lower three panels). Upper panel, left: 3D model of *G*-1**a** (top), *G*-2**a** (middle), and *G*-3**a** (bottom); right: corresponding molecular surfaces. Lower panel, left: 3D model of *G*-1**b** (top), *G*-2**b** (middle), and *G*-3**b** (bottom); right: relative molecular surfaces. Atom color code for 3D models: carbon = gray; hydrogen = white; nitrogen = blue; oxygen = red. Models on right are not scaled to point out the characteristics of molecular surfaces.

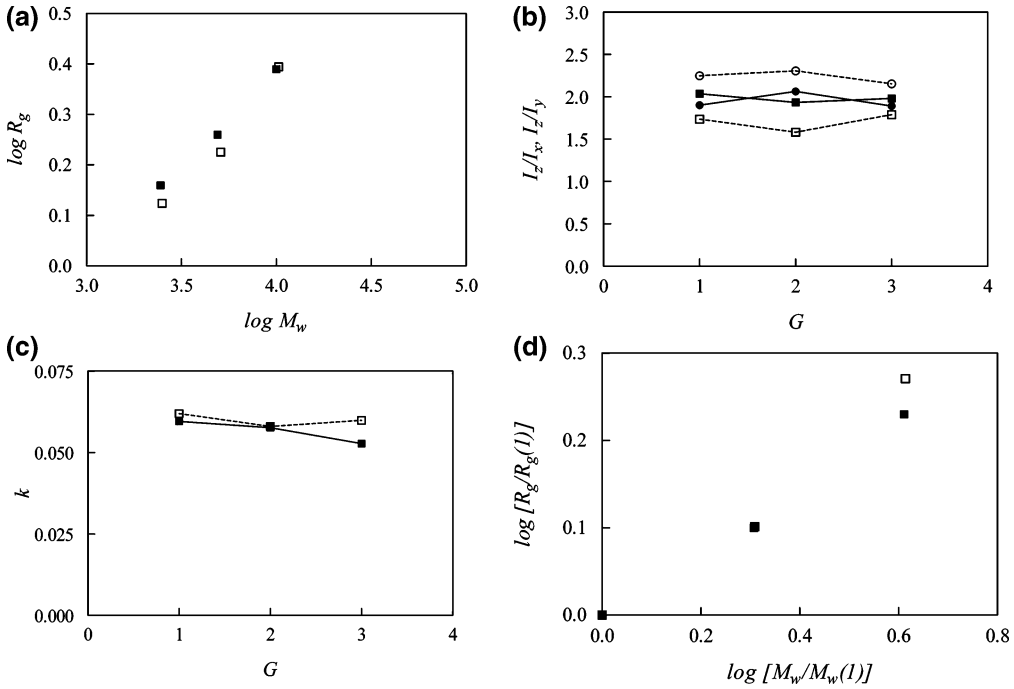

Figure 5. (a) Relationship between radius of gyration R_g and molecular weight M_w for both dendrimer families. Filled symbols: **a**; open symbols: **b**. (b, middle) Average aspect ratios I_z/I_x and I_z/I_y for the three generations of dendrimers **a** and **b**. Filled symbols: **a**; open symbols: **b**. Symbol legend: squares = I_z/I_x; circles = I_z/I_y. (c, middle) Relative shape anisotropy k for the three generations of dendrimers **a** and **b**. Filled symbols: **a**; open symbols: **b**. (d) Relationship between normalized radius of gyration $R_g/R_g(1)$ and normalized molecular mass $M_w/M_w(1)$ for both dendrimer families. Filled symbols: **a**; open symbols: **b**. Lines are only a guideline for the eye.

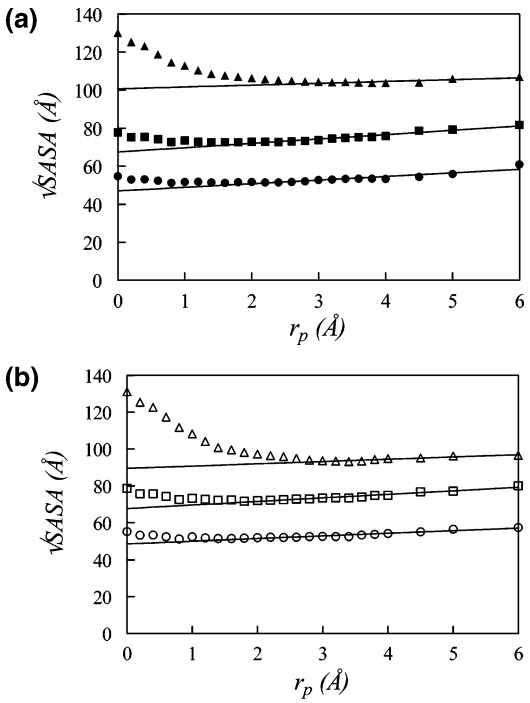

Figure 6. Plots of √SASA as a function of the probe radius r_p for the three generations of dendrimers **a** (a, top) and **b** (b, bottom). Filled symbols: **a**; open symbols: **b**; lines: linear regression. Symbol legend: circles = *G*-1; squares = *G*-2; triangles, *G*-3.

where R is the radius of ideally spherical molecule, and r_p is the radius of the probe. For such a molecule, a plot of $(V_{SASA})^{1/3}$ versus r_p would be linear with a slope of $(^4/_3\pi)^{1/3}$ and intercept proportional to the radius R. Indeed, in the case of both dendrimers **a** and **b**, eq 12 is satisfied for large probe radii, but there is a deficit of volume for small probes, owing to the presence of the internal cavities and channels, as shown in Figure 7a,b. The estimated fraction of internal volume, V_{int}, ranges from approximately 17% of *G*-1 to 22% of *G*-3, as listed in Table 2. Once again, this behavior is utterly similar to that exhibited by other dendrimeric families.[5,33,52]

Table 2. van der Waals Molecular Surface Area (A_{vdW}) and Volume (V_{vdW}), Fraction of Internal Surface Area (A_{int}), Fraction of Internal Volume (V_{int}), Dimensions of the Dendrimers d_{SASA}, d_{VSASA}, and Maximum Diameter d_{max} for Both Dendrimer Series

dendrimer	A_{vdW} (nm^2)	V_{vdW} (nm^3)	A_{int} (%)	d_{SASA} (nm)	V_{int} (%)	d_{VSASA} (nm)	d_{max} (nm)
G-1**a**	29.0	2.5	15	3.99	17	4.10	4.53 ± 0.10
G-2**a**	58.5	5.1	16	5.53	19	5.62	5.97 ± 0.09
G-3**a**	117.1	10.3	29	6.94	20	7.05	7.20 ± 0.11
G-1**b**	29.4	2.6	14	4.19	18	4.35	4.28 ± 0.15
G-2**b**	59.6	5.1	16	5.13	19	5.01	5.31 ± 0.10
G-3**b**	120.1	10.5	46	5.41	22	5.58	5.52 ± 0.05

The MD simulations data were also used to estimate the size ("effective limiting diameters") of both series of dendrimers **a** and **b** as a function of *G* (see Table 2). Three quantities were calculated from these in silico experiments: (i) d_{SASA}, the molecular diameter determined from the linear regression fits of √SASA vs r_p, (ii) d_{VSASA}, the molecular diameter determined from the linear regression fits of $(V_{SASA})^{1/3}$ vs r_p, and (iii) d_{max}, the maximal end-to-end distance between terminal heteroatoms. This last quantity was determined periodically and averaged over the entire set of MD trajectories, and its value should in principle provide an upper bound because it emphasizes any dangling arms protruding out of the dendrimer. Generally speaking, as we can infer from a global analysis of data in Table 2, there is a very good agreement between all values calculated from different evidence, and the d_{max} indeed provides an upper bracket to the other calculated diameters.

The degree of geometric irregularity of a dendrimer is one of the parameters that determines the diffusion kinetics of a small substrate on the surface of the macromolecule or into it. The degree of irregularity of a surface may be described by means of a fractal dimension d_f.[53]

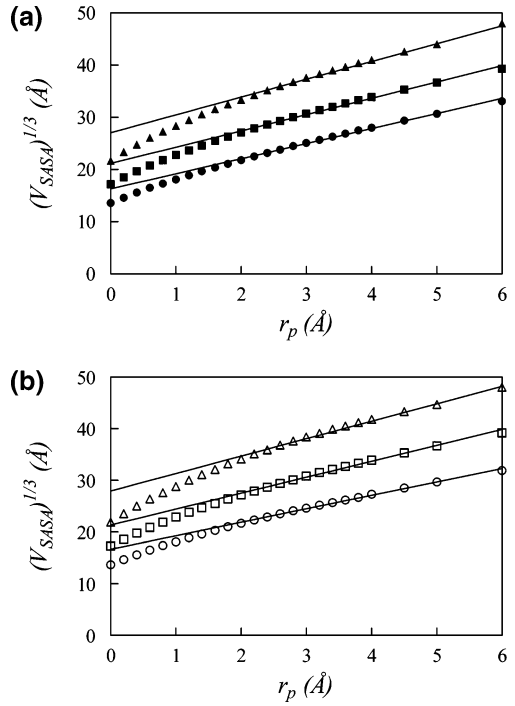

Figure 7. Plots of $(V_{SASA})^{1/3}$ as a function of the probe radius r_p for the three generations of dendrimers **a** (a, top) and **b** (b, bottom). Filled symbols: **a**; open symbols: **b**; lines: linear regression. Symbol legend: circles = *G*-1; squares = *G*-2; triangles, *G*-3.

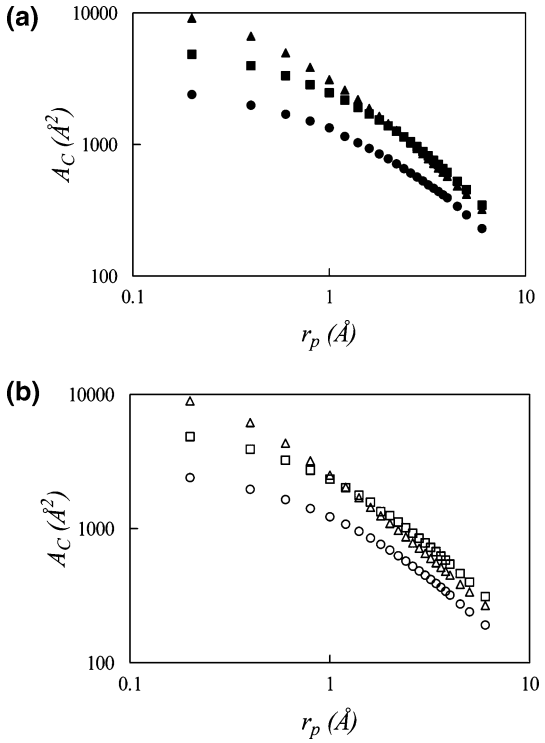

Figure 8. Plots of A_c as a function of the probe radius r_p for the three generations of dendrimers **a** (a, top) and **b** (b, bottom). Filled symbols: **a**; open symbols: **b**; lines: linear regression. Symbol legend: circles = *G*-1; squares = *G*-2; triangles, *G*-3.

According to a known, validated procedure,[31−34,52] the value of d_f, usually interpreted as the fractal dimension of the surface available to adsorption, may be obtained from the slope of the $\log(A_C) - \log(r_p)$ curve as follows:

$$2 - d_f = \frac{d\log(A_C)}{d\log(r_p)} \tag{13}$$

A_C is the contact component of the Connolly molecular surface.[36−38] According to this definition, the molecular surface consists of the van der Waals surface of the atoms that can be touched by a solvent-sized probe sphere (thus called *contact surface*), connected by a network of concave and saddle surfaces (globally called *reentrant surface*). Thus, A_C accounts for the superficial contacts between different macromolecules. Consequently, d_f gives information concerning the surface roughness and accessibility of macromolecules. Indeed, according to its definition, as a molecular surface becomes more irregular, the corresponding fractal dimension increases, starting from its lower value $d_f = 2$, equivalent to an entirely smooth surface, up to an extreme, volumelike irregularity ($d_f = 3$). Parts a and b of Figure 8 report the $\log(A_C) - \log(r_p)$ curves obtained for the three dendrimer generations of **a** and **b**.

As we may infer from these graphs, the slopes of the plots show a tendency to reach a plateau, corresponding to $d_f = 2$, in the limit of small probe size. Small probes predominantly interact with the smooth van der Waals spheres describing the dendrimer atom; for probes of intermediate dimensions, the values of *D* are in the range of 2.4−2.6 Å for both families and increase with the generational growth. It is important to note that the value of *D* is quite similar for each generation, independently of the chemical nature of the internal branches, as highlighted in Table 3 and in harmony with the fractal dimension values derived from the dependence of R_g vs M_w (vide supra).

Table 3. Surface Fractal Dimension d_f for the Three Generations of Dendrimers a and b

dendrimer	*G*-1	*G*-2	*G*-3
a	2.44	2.53	2.62
b	2.54	2.58	2.63

As mentioned earlier, parameters such as size, shape, and multiplicity are transcribed and displayed throughout the dendrimer growth. These variables can have dramatic effects on the ultimate shape, the interior topology, and the exterior surface properties (alias *congestion*) of the developing molecule. Mathematically, we can appraise dendrimer surface congestion as a function of generation from eq 14:

$$A_Z = \frac{A}{N_Z} \propto \frac{R^2}{N_c N_b^G} \tag{14}$$

in which A_Z is the surface area per terminal group *Z*, *A* is the dendrimer surface area, and N_Z is the number of terminal groups *Z* per generation.[5] From this relation we can see that, at higher generations of *G*, the surface area per *Z* group should become increasingly smaller and experimentally approach the cross-sectional area of the van der Waals dimension of the surface group *Z*. The generation *G* thus reached is referred to as the starburst dense-packed (limited) generation. As predicted by de Gennes and Hervet,[54] ideal starburst growth without branch defects is possible only for those generations preceding the dense-packed state. This critical dendrimer property gives rise to self-limiting starburst dimensions, which are a function of the branch-segment length *L*, the core multiplicity N_c, the branch-juncture multiplicity N_b, and the sterical dimensions of the terminal group *Z*. Because the dendrimer radius *R* in the expression above is dependent on *L*, larger *L* values will delay this congestion, whereas larger N_c and N_b values and larger *Z* dimensions will dramatically hasten it.

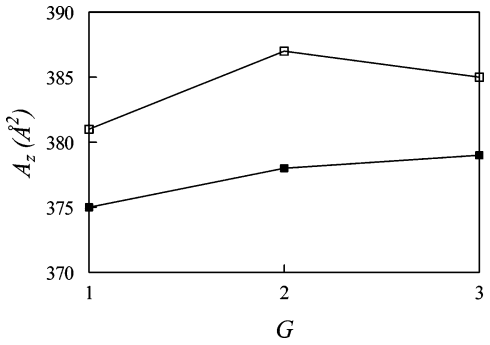

Figure 9. Surface area per terminal group A_z vs generation G for the two dendrimer series. Filled symbols, **a**; open symbols, **b**.

Computer-assisted molecular simulations allowed us to determine the surface area per Z group, A_Z, as a function Z of generation for all series, as shown in Figure 9; we used the first relation in eq 14.

As can be seen in Figure 9, for all dendrimer families, A_Z increases from generation 1 to 2, but albeit for family **a**, there is only a change in the rate of increase at G-3 for the molecules of series **b**. A_z presents a maximum at G-2 and then decreases, owing to the beginning of the surface congestion. Accordingly, this analysis allows us to conclude that, for this type of dendrimer, the starburst-limited generation, that is the generation at which the molecule should exhibit sterically inhibited reaction rates and sterically induced stoichiometry, is presumably located in correspondence of G-3 for the molecules of series **a** and of G-2 for the alternative series **b**.

Free Energy of Binding of Compounds c and d by Dendrimers a and b. The application of the MM/PBSA protocol allowed us to estimate the free energy of binding, ΔG_{BIND}, of small molecules such as compounds **c** and **d**, to all three generations of dendrimers **a** and **b**. Figure 10 shows MD-equilibrated snapshots of each molecular complex, while Tables 4 and 5 list the corresponding values of ΔG_{BIND} and all its components.

The statistical analysis of our calculated data sets reveals a good correlation for the MM/PBSA ΔG_{BIND} of all complexes considered with experiment. In fact, the small value of the root-mean-square deviation (0.28) or, equivalently, of the mean relative deviation modulus (defined as $\sum_i$ [|(exp − calc)/exp|/N] × 100) (3%) indicate an accurate reproduction of free energy of binding by this technique. This is especially encouraging for dendrimer host−small molecule guest complexes, also because sufficient conformational sampling might be a challenge for flexible dendrimeric molecules and because of different dendrimer architectural features.

Further insight into the forces involved in guest binding can be obtained by analyzing the MM/PBSA free energy contributions, also listed in Tables 4 and 5. For both series of dendrimers, the intermolecular van der Waals and the electrostatics are both important contribution to the binding. However, the electrostatic desolvation penalty (ΔG_{ELE}^{SOLV}) offsets the favorable (negative) intermolecular electrostatics, yielding an unfavorable net electrostatic contribution to the binding. Generally speaking, both compounds **c** and **d** form several, persistent hydrogen bonds with the nitrogen atoms of the dendrimer common core, and the intermolecular electrostatics interactions are accordingly rather strong. However, the desolvation penalty upon binding for these two molecules is quite large; thereby, the net electrostatic contributions to the binding (i.e., $\Delta E_{ELE}^{MM} + \Delta G_{ELE}^{SOLV}$) for these compounds are significantly unfavorable. Comparing the van der Waals/nonpolar terms ($\Delta E_{vDW}^{MM} + \Delta G_{NP}^{SOLV}$) with the electrostatic contributions ($\Delta E_{ELE}^{MM} + \Delta G_{ELE}^{SOLV}$) we can see that the association between all dendrimers and their guest is then mainly driven by more favorable nonpolar interactions in the complex than in solution, independently of the nature of the dendrimer branches and of dendrimer genera-

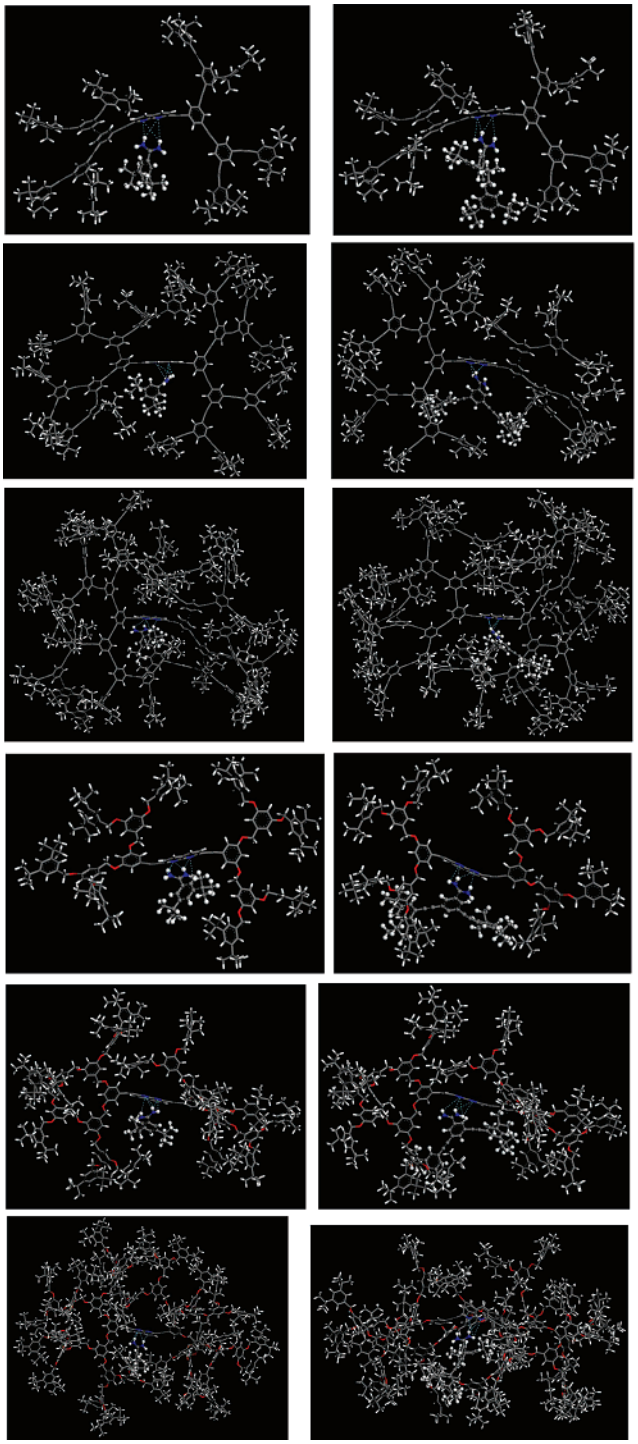

Figure 10. Molecular models of the inclusion complexes taken from equilibrated MM/PBSA MD snapshots for dendrimers **a** (upper six panels) and dendrimers **b** (lower six panels). Upper panels: 3D models of **a** G-1**c** (top, left), (top), **a** G-1**d** (top, right), **a** G-2**c** (middle, left), **a** G-2**d** (middle, right), and **a** G-3**c** (bottom, left), **a** G-3**d** (bottom, right). Lower panels: 3D model of **b** G-1**c** (top, left), **b** G-1**d** (top, right), b**2** G-2**c** (middle, left), **b** G-2**d** (middle, right), and **b** G-3**c** (bottom, left), **b** G-3**d** (bottom, right). Atom color code for 3D models: carbon = gray; hydrogen = white; nitrogen = blue; oxygen = red. Hydrogen bonds are depicted as cyan broken lines. Models are not scaled in order to point out the binding at the core.

Table 4. Free Energy of Binding for Compounds c with Dendrimers a and b[a]

	ΔE_{vDW}^{MM}	ΔE_{ELE}^{MM}	ΔG_{ELE}^{SOLV}	ΔG_{NP}^{SOLV}	$-T\Delta S$	ΔG_{BIND}	$\Delta G_{BIND,exp}$
G-1**a**	-41.3 ± 0.3	-29.3 ± 0.5	60.2 ± 0.4	-3.5 ± 0.1	10.1 ± 0.9	-3.9 ± 0.7	-3.9
G-2**a**	-40.2 ± 0.4	-30.4 ± 0.5	59.5 ± 0.4	-3.7 ± 0.1	10.6 ± 0.8	-4.1 ± 0.7	-3.7
G-3**a**	-39.3 ± 0.6	-30.3 ± 0.6	58.3 ± 0.5	-3.9 ± 0.1	11.1 ± 0.9	-4.0 ± 0.8	-3.5
G-1**b**	-40.0 ± 0.3	-31.5 ± 0.5	60.3 ± 0.5	-3.6 ± 0.1	10.6 ± 0.8	-4.2 ± 0.7	-4.2
G-2**b**	-40.4 ± 0.3	-30.2 ± 0.5	59.4 ± 0.4	-3.8 ± 0.1	10.9 ± 0.8	-4.0 ± 0.7	-4.1
G-3**b**	-40.0 ± 0.7	-31.7 ± 0.7	60.0 ± 0.6	-3.9 ± 0.1	11.4 ± 0.9	-4.2 ± 0.8	-3.6

[a] All energy values are expressed in kcal/mol. Experimental values from ref 23.

Table 5. Free Energy of Binding for Compounds d with Dendrimers a and b[a]

	ΔE_{vDW}^{MM}	ΔE_{ELE}^{MM}	ΔG_{ELE}^{SOLV}	ΔG_{NP}^{SOLV}	$-T\Delta S$	ΔG_{BIND}	$\Delta G_{BIND,exp}$
G-1**a**	-39.3 ± 0.4	-30.2 ± 0.6	57.0 ± 0.5	-5.8 ± 0.1	14.7 ± 0.8	-3.7 ± 0.7	-3.9
G-2**a**	-40.1 ± 0.4	-31.0 ± 0.5	57.8 ± 0.4	-6.0 ± 0.1	15.3 ± 0.9	-3.9 ± 0.6	-3.9
G-3**a**	-38.3 ± 0.3	-32.1 ± 0.5	56.3 ± 0.6	-6.0 ± 0.1	16.2 ± 0.9	-3.9 ± 0.8	-3.9
G-1**b**	-39.1 ± 0.4	-33.0 ± 0.4	60.1 ± 0.6	-5.9 ± 0.1	14.0 ± 0.7	-4.0 ± 0.8	-4.2
G-2**b**	-41.1 ± 0.3	-32.3 ± 0.6	59.4 ± 0.5	-5.9 ± 0.1	16.0 ± 0.8	-3.9 ± 0.7	-4.0
G-3**b**	-41.9 ± 0.5	-33.3 ± 0.7	61.2 ± 0.6	-6.0 ± 0.1	15.9 ± 0.7	-4.1 ± 0.8	-3.9

[a] All energy values are expressed in kcal/mol. Experimental values from ref 23.

tion. Finally, also the calculated changes in solute entropy, $-T\Delta S$, are physically reasonable, with the more rigid molecular scaffold characterizing compound **d** revealing a higher change in solute entropy upon binding.

It is particularly encouraging for our procedure that the large van der Waals contribution to ΔG_{BIND} is compensated sensibly by the other contributions, globally resulting in only slight deviations from experiment. In fact, for a given guest, the practically constant value of the free energy of binding between the two different dendrimeric series **a** and **b** with respect to guest molecules **c** and **d** is mainly due to the fact that the outer dendrimeric parts mainly contribute to create an apolar microenvironment for binding, while main host−guest interactions take place at the common, more polar dendrimer core, in perfect agreement with the corresponding experimentally based speculations.

Conclusions

Host−guest interaction and complexation in a dendritic architecture are intriguing properties of dendrimers. Given the chemical nature and structure of their cores branches, dendrimers adopt shapes in solutions that may allow for their cores to be relatively loosely linked and have enough space to encapsulate small molecules. One of the most characteristic features of dendrimers is that, by increasing generation, controlled cavities can develop, again depending on chemical composition, branch flexibility, and number of branching arms at junction points. Another intriguing aspect is that functional units involving ligands can be placed in planned sites in dendrimers (e.g., core or surface), which is profitable to construct functionalized materials required for vectorial interaction. In contrast to nonspecific physical encapsulation of guest molecules within the dendritic branches, the location of small molecules can be controlled by the incorporation of specific binding sites utilizing hydrophobic interactions, hydrogen bonding, and a metal ion coordination site. Among these, hydrogen-bonding sites within dendrimer frameworks have been proven to be powerful tools as a predetermined place for binding of guest molecules; in particular, the effects of different branch units stemming from a common core in dendritic molecules **a** and **b** on the complexation behavior based on hydrogen bonding between the core and two different guest molecules **c** and **d** have been studied by Zimmerman et al.[23] For both guest molecules **c** and **d**, these authors found that the stoichiometry of the relevant complexes was 1:1 and that the binding constants between dendritic host and small guest were almost independent of the nature of the dendrimer branch and, even more interesting, of dendrimer generation. Accordingly, they concluded that both guests were trapped at the dendrimer common naphthyridine core, and that these compounds could penetrate into the dendrimer structure without any specific chemical and physical interaction of framework.

Our molecular characterization of the first three generations of both dendrimer series **a** and **b** (the former characterized by apolar phenylacetylene branches, and the latter bearing more polar oxymethylene units), performed via molecular modeling and simulations, revealed that the geometry of the core strongly influences the generational growth of these macromolecules, ultimately resulting in similar, flowerlike, shape-consistent macromolecular hosts. In these structures, the naphthyridine moiety remains relatively available for complexation by virtue of a central cavity of characteristic dimensions of about 13 Å, generated and maintained near the core for both dendrimer classes and generations.

The calculations of the free energies of binding between all dendrimers and their guests, obtained by applying the so-called MM/PBSA methodology, are in utter agreement with the corresponding experimental values. The analysis of the relevant MD trajectories revealed that indeed the major intermolecular forces holding all complexes together are found in the formation of several, persistent hydrogen bonds between the guests and the dendrimer core, as well as in the favorable nonpolar microenvironment generated by the dendrimeric branches around the binding cavity.

The properties of shape persistency with controlled size are extremely useful in the area of nanotechnology. The functionality of dendrimers that have been described in this paper might be amplified by more judicious choice of the core, building block, and terminal units according to research needs. In this respect, the ability of molecular simulations to unveil the major structural characteristics of dendrimers, such as the (quali)-quantification of internal voids, fractal dimensions, shape persistency, etc., coupled with the capacity of the MM/PBSA approach to quantitatively predict the free energy of binding between dendrimeric host and small guest, constitute a promising step toward a more accurate theoretical description of host/guest complexes and, consequently, a faster and better new supramolecular system design.

References and Notes

(1) Buhleier, E.; Wehner, W.; Vögtle, F. *Synthesis* **1978**, *2*, 155−158.

(2) Tomalia, D. A.; Baker, H.; Dewald, J. R.; Hall, M.; Kallos, G.; Martin, S.; Roeck, J.; Ryder, J.; Smith, P. *Polym. J.* **1985**, *17*, 117−132.
(3) Tomalia, D. A.; Baker, H.; Dewald, J. R.; Hall, M.; Kallos, G.; Martin, S.; Roeck, J.; Ryder, J.; Smith, P. *Macromolecules* **1986**, *19*, 2466−2468.
(4) Newkome, G. R.; Yao, Z.-Q.; Baker, G. R.; Gupta, V. K. *J. Org. Chem.* **1985**, *50*, 2003−2004.
(5) Tomalia, D. A.; Naylor, A. M.; Goddard, W. A., III. *Angew. Chem., Int. Ed. Engl.* **1990**, *29*, 138−175.
(6) Tomalia, D. A. *Sci. Am.* **1995**, *272*, 62−66.
(7) Newkome, G. R.; Moorfield, C. N.; Vögtle, F. *Dendritic Molecules*; VCH: Weinheim, Germany, 1996.
(8) Fréchet, J. M. J. *Science* **1994**, *263*, 1710−1715.
(9) Zeng, F.; Zimmerman, S. C. *Chem. Rev.* **1997**, *97*, 1681−1712.
(10) Tomalia, D. A. *Adv. Mater.* **1994**, *6*, 529−539.
(11) Wilkinson, M. J.; van Leeuwen, P. W. N. M.; Reek, J. N. H. *Org. Biol. Chem.* **2005**, *3*, 2371−2383.
(12) Bosman, A. W.; Janssen, H. M.; Meijer, E. W. *Chem. Rev.* **1999**, *99*, 1665−1688.
(13) Smith, D. K.; Diederich, F. *Chem.—Eur. J.* **1998**, *4*, 1353−1361.
(14) Gillies, E. R.; Frechet, J. M. *Drug Discovery Today* **2005**, *10*, 35−43.
(15) Caruthers, S. D.; Winter, P. M.; Wickline, S. A.; Lanza, G. M. *Methods Mol. Med.* **2006**, *124*, 387−400.
(16) Hilgenbrink, A. R.; Low, P. S. *J. Pharm. Sci.* **2005**, *94*, 2135−2146.
(17) Dufes, C.; Uchegbu, I. F.; Schatzlein, A. G. *Adv. Drug Delivery Rev.* **2005**, *57*, 2177−2202.
(18) Kofoed, J.; Reymond, J. L. *Curr. Opin. Chem. Biol.* **2005**, *9*, 656−664.
(19) Balzani, V.; Ceroni, P.; Maestri, M.; Vicinelli, V. *Curr. Opin. Chem. Biol.* **2003**, *7*, 657−665.
(20) Tomalia, D. A.; Uppuluri, S.; Swanson, D. R.; Li, L. *Pure Appl. Chem.* **2000**, *72*, 2343−2358.
(21) Jansen, J. F. G. A.; de Brabander-van den Berg, E. M. M.; Meijer, E. W. *Science* **1994**, *266*, 1226−1229.
(22) Liu, M.; Fréchet, J. M. J. *Pharm. Sci. Technol. Today* **1999**, *2*, 393−401.
(23) Zimmerman, S. C.; Wang, Y.; Bharathi, P.; Moore, J. S. *J. Am. Chem. Soc.* **1998**, *120*, 2172−2173.
(24) Srinivasan, J.; Cheatham, T. E., III; Cieplak, P.; Kollman, P. A.; Case, D. A. *J. Am. Chem. Soc.* **1998**, *120*, 9401.
(25) Pearlman, D. A.; Case, D. A.; Caldwell, J. W.; Ross, W. S.; Cheatham, T. E., III; DeBolt, S.; Ferguson, D.; Seibel, G.; Kollman, P. A. *Comp. Phys. Commun.* **1995**, *91*, 1−41.
(26) Case, D. A.; Pearlman, D. A.; Caldwell, J. W.; Cheatham, T. E., III; Wang, J.; Ross, W. S.; Simmerling, C. L.; Darden, T. A.; Merz, K. M.; Stanton, R. V.; Cheng, A. L.; Vincent, J. J.; Crowley, M.; Tsui, V.; Gohlke, H.; Radmer, R. J.; Duan, Y.; Pitera, J.; Massova, I.; Seibel, G. L.; Singh, U. C.; Weiner, P. K.; Kollman, P. A. *AMBER 7*; University of California: San Francisco, 2000.
(27) Wang, J.; Cieplak, P.; Kollman, P. A. *J. Comput. Chem.* **2000**, *21*, 1049−1074.
(28) Dewar, M. J. S.; Zoebisch, E. G.; Healy, E. F.; Stewart, J. J. P. *J. Am. Chem. Soc.* **1985**, *107*, 3902−3909.
(29) Bayly, C. I.; Cieplak, P.; Cornell, W. D.; Kollman, P. A. *J. Phys. Chem.* **1993**, *97*, 10269−10280.
(30) Wang, J.; Wang, W.; Kollman, P. A.; Case, D. A. *J. Comput. Chem.* **2005**, *25*, 1157−1174.
(31) Pricl, S.; Fermeglia, M. *Carbohydr. Polym.* **2001**, *45*, 23−33.
(32) Fermeglia, M.; Ferrone, M.; Pricl, S. *Bioorg. Med. Chem.* **2002**, *10*, 2471−2478.
(33) Pricl, S.; Fermeglia, M.; Ferrone, M.; Asquini, A. *Carbon* **2003**, *41*, 2269−2283.
(34) Metullio, L.; Ferrone, M.; Coslanich, A.; Fuchs, S.; Fermeglia, M.; Paneni, M. S.; Pricl, S. *Biomacromolecules* **2004**, *5*, 1371−1378.
(35) Jayaram, B.; Sprous, D.; Beveridge, D. L. *J. Phys. Chem.* **1998**, *102*, 9571−9576.
(36) Connolly, M. L. *J. Appl. Crystallogr.* **1983**, *16*, 548−558.
(37) Connolly, M. L. *Science* **1983**, *221*, 709−713.
(38) Connolly, M. L. *J. Am. Chem. Soc.* **1985**, *107*, 1118−1124.
(39) Lee, B.; Richards, F. M. *J. Mol. Biol.* **1971**, *55*, 379−400.
(40) Richards, F. M. *Annu. Rev. Biophys. Bioeng.* **1977**, *6*, 151−176.
(41) Felluga, F.; Fermeglia, M.; Ferrone, M.; Pitacco, G.; Pricl, S.; Valentin, E. *Tetrahedron: Asymmetry* **2002**, *13*, 475.
(42) Felluga, F.; Pitacco, G.; Valentin, E.; Coslanich, A.; Fermeglia, M.; Ferrone, M.; Pricl, S. *Tetrahedron: Asymmetry* **2003**, *14*, 3385−3399.
(43) Frecer, V.; Kabelac, M.; De Nardi, P.; Pricl, S.; Miertus, S. *J. Mol. Graphics Modell.* **2004**, *22*, 209.
(44) Fermeglia, M.; Ferrone, M.; Tamborini, E.; Pricl, S. *Mol. Cancer Ther.* **2005**, *4*, 1167−1174.
(45) Tamborini, E.; Pricl, S.; Negri, T.; Lagonigro, M. S.; Piselli, F.; Greco, A.; Gronchi, A.; Casali, P.; Ferrone, M.; Fermeglia, M.; Pienotti, M. A.; Pilotti, S. *Oncogene* **2006**, *25*, 6140−6146.
(46) Gilson, M. K.; Sharp, K. A.; Honig, B. H. *J. Comput. Chem.* **1987**, *9*, 327−335.
(47) Sanner, M. F.; Olson, A. J.; Spehner, J. C. *Biopolymers* **1996**, *38*, 305−320.
(48) Wilson, E. B.; Decius, J. C.; Cross, P. C. *Molecular Vibrations*; McGraw-Hill: New York, 1955.
(49) Morgenroth, F.; Kübel, C.; Müller, M.; Wiesler, U. M.; Berresheim, A. J.; Wagner, M.; Müllen, K. *Carbon* **1998**, *36*, 833−837.
(50) Brocorens, P.; Zojer, E.; Cornil, J.; Shuai, Z.; Leising, G.; Müllen, K.; Brédas, J. L. *Synth. Met.* **1999**, *100*, 141−162.
(51) Theodorou, D. N.; Suter, U. W. *Macromolecules* **1985**, *18*, 1206−1214.
(52) Blasizza, E.; Fermeglia, M.; Pricl, S. *Mol. Simul.* **2000**, *24*, 167−189.
(53) Mandelbrot, B. B. *The Fractal Geometry of Nature*; Freeman: San Francisco, 1983.
(54) de Gennes, P. G.; Hervet, H. J. *J. Phys. Lett.* **1983**, *44*, 351−360.

MA062610A